Through-space 11 B– 27 Al correlation: Influence of the recoupling channel

Mingji Zheng, Shaohui Xin, Qiang Wang, Julien Trébosc, Jun Xu, Guodong Qi, Ningdong Feng, Olivier Lafon, Feng Deng

▶ **To cite this version:**

Mingji Zheng, Shaohui Xin, Qiang Wang, Julien Trébosc, Jun Xu, et al.. Through-space 11 B– 27 Al correlation: Influence of the recoupling channel. Magnetic Resonance in Chemistry, 2021, 59 (9-10), pp.1062-1076. 10.1002/mrc.5163 . hal-03402966

HAL Id: hal-03402966
https://hal.science/hal-03402966v1

Submitted on 25 Oct 2021

HAL is a multi-disciplinary open access archive for the deposit and dissemination of scientific research documents, whether they are published or not. The documents may come from teaching and research institutions in France or abroad, or from public or private research centers.

L'archive ouverte pluridisciplinaire **HAL**, est destinée au dépôt et à la diffusion de documents scientifiques de niveau recherche, publiés ou non, émanant des établissements d'enseignement et de recherche français ou étrangers, des laboratoires publics ou privés.

Through-space ^{11}B-^{27}Al Correlation: influence of the recoupling channel

Mingji Zheng,[a,c]† Shaohui Xin,[a,d]† Qiang Wang,[a]* Julien Trébosc,[b,f] Jun Xu,[a] Guodong Qi,[a] Ningdong Feng,[a] Olivier Lafon[b,e]* and Feng Deng[a]*

a. *National Centre for Magnetic Resonance in Wuhan, State Key Laboratory of Magnetic Resonance and Atomic and Molecular Physics, Innovation Academy for Precision Measurement Science and Technology, Chinese Academy of Sciences, Wuhan 430071, China.*
b. *Univ. Lille, CNRS, Centrale Lille, Univ. Artois, UMR 8181 – UCCS –, Unité de Catalyse et de Chimie du Solide, F- 59000 Lille, France*
c. *University of Chinese Academy of Sciences, Beijing 100049*
d. *Wanhua Chemical Group Co.,Ltd,*
e. *Institut Universitaire de France, 75231 Paris, France*
f. *Univ. Lille, CNRS, INRA, Centrale Lille, Univ. Artois, FR 2638 - IMEC - Institut Michel-Eugène Chevreul, F-59000 Lille, France*

†. Authors with equal contributions

Email: qiangwang@wipm.ac.cn; olivier.lafon@univ-lille.fr; dengf@wipm.ac.cn

Abstract

Through-space heteronuclear correlation (*D*-HETCOR) experiments based on heteronuclear multiple-quantum correlation (*D*-HMQC) or refocused insensitive nuclei enhanced by polarization transfer (*D*-RINEPT) sequences prove to be useful approaches for the NMR detection of the spatial proximity between half-integer quadrupolar nuclei in solids under magic-angle spinning (MAS) conditions. These sequences employ coherence transfers mediated by heteronuclear dipolar interactions, which are reintroduced under MAS by radiofrequency irradiation of only one of the two correlated nuclei. We investigate herein using numerical simulations of spin dynamics and solid-state NMR experiments on magnesium aluminoborate glass how the choice of the channel to which the heteronuclear dipolar recoupling is applied affects the transfer efficiency of *D*-HMQC and *D*-RINEPT sequences between ^{11}B and ^{27}Al nuclei. Experimental results show that maximum transfer efficiency is achieved

when the recoupling scheme is applied to the channel, for which the nuclear magnetization points towards the B_0 axis in average.

1. Introduction

Half-integer quadrupolar nuclei, such as ^{27}Al (I = 5/2), ^{17}O (I = 5/2), ^{11}B (I = 3/2), ^{23}Na (I = 3/2), $^{67/71}$Ga (I = 3/2) and ^{67}Zn (I = 5/2), represent about two thirds of stable NMR-active nuclei and are present in a broad range of materials, including zeolites,[1-2] supported catalysts, geopolymers,[3] ceramics,[4-5] glasses,[6-7] energy materials, pharmaceuticals, biological molecules.[8-9] Over half a century, considerable effort has been oriented towards methodological developments for the NMR observation of these quadrupolar nuclei in solids,[10-15] which have provided new insights into atomic scale structure of materials.[16-23]

In particular, proximities between distinct half-integer quadrupolar isotopes, such as ^{27}Al and ^{11}B, ^{27}Al and ^{17}O or ^{11}B and ^{23}Na, in solids have been probed using cross-polarization under magic-angle spinning (CPMAS) transfer using continuous-wave (CW) irradiation[24-26] or a train of a rotor-synchronized pulses.[27] However, these techniques lack of robustness owing to the difficulty to spin lock the magnetization of the two quadrupolar isotopes under magic-angle spinning (MAS) conditions.[28-31] More recently we have demonstrated that proximities between distinct half-integer quadrupolar isotopes in solids can be probed using dipolar-based heteronuclear multiple-quantum coherence (*D*-HMQC) and dipolar-based refocused insensitive nuclei enhanced by polarization transfer (*D*-RINEPT) methods[32], which have previously been successfully employed to correlate the NMR signals of spin-1/2 and quadrupolar nuclei. [12, 33-44] These sequences benefit from improved robustness with respect to CPMAS transfer since the dipolar interactions between distinct half-integer quadrupolar nuclei are reintroduced by the application of radiofrequency (rf) fields to only one of the correlated isotopes, instead of two in the case of CPMAS technique. These *D*-HMQC and *D*-RINEPT techniques have been applied to correlate the central transitions (CTs) of two distinct half-integer quadrupolar nuclei, ^{23}Na (I = 3/2) and ^{27}Al

(I = 5/2), having close Larmor frequencies in heterogeneous catalysts Na_2CO_3/γ-Al_2O_3.[32] The ^{23}Na-^{27}Al dipolar interactions have been reintroduced by the application of low-power symmetry-based heteronuclear dipolar recoupling schemes, such as $SR4_1^2$,[45] $R2_1^1$ [46] and synchronous phase inversion rotary resonance recoupling (SPI-R^3) [47-48] .

In this contribution, we investigate how the choice of the channel to which the heteronuclear dipolar recoupling is applied affects the efficiency of coherence transfer of *D*-HMQC and *D*-RINEPT schemes between two different half-integer quadrupolar spins. This study is performed in the case of ^{11}B (I = 3/2) and ^{27}Al (I = 5/2) using numerical simulations of spin dynamics as well as solid-state NMR experiments on magnesium aluminoborate glass. The ^{11}B-^{27}Al dipolar interactions are reintroduced under MAS conditions using SPI-R^3 scheme, for which the nutation frequency of the CT is equal to the MAS frequency, ν_R. This recoupling scheme corresponds to the $C2_2^1$ symmetry.[49]

2. Methods

2.1 Pulse sequence

In the $S\{I\}$ *D*-HMQC sequence, shown in Fig. 1, the dipolar recoupling sequence can be applied to the detected spy spin S (Fig. 1a, denoted as D^S-HMQC) or indirectly detected spin I (Fig. 1b, denoted as D^I-HMQC)[36] to restore the heteronuclear dipolar dephasings under MAS. Fig. 1c displays the SPI-R^3 heteronuclear recoupling scheme. This scheme consists of a train of CT-selective 2π pulses with opposite phases (y and $-y$) with a nutation frequency of the CT, ν_{nut}, equal to ν_R.

In the case of $S\{I\}$ *D*-RINEPT sequence, the recoupling schemes can be applied either to the S or I spins during the defocusing and refocusing delays independently. The corresponding four *D*-RINEPT variants, denoted *II*, *SS*, *IS* and *SI*, are displayed in Figs. 2a to d, respectively.

In addition, for both *D*-HMQC and *D*-RINEPT sequences, the S spin could be either ^{11}B or ^{27}Al. Furthermore, the initial CT polarization of S spins could be enhanced by the saturation or inversion of their satellite transitions by the application of schemes, such as double frequency sweep (DFS) scheme,[50-51] hyperbolic secant (HS) pulse,[52-53]

fast amplitude modulated (FAM) pulses, also named rotor-assisted population transfer (RAPT)[54-56] and quadruple frequency sweep (QFS)[57].

2.2 Numerical Simulations

Simulations of spin dynamics during *D*-HMQC and *D*-RINEPT sequences were performed using the SIMPSON software (version 4.2.1)[58] and a ^{11}B-^{27}Al spin pair. The powder averaging was accomplished using 3384 Euler orientations: 376 $\{\alpha_{MR}, \beta_{MR}\}$-pairs and 9 γ_{MR}-angles. The 376 $\{\alpha_{MR}, \beta_{MR}\}$-pairs, which relate the molecular and rotor frames, were selected according to the ZCW algorithm.[59-60] For all *D*-HMQC and *D*-RINEPT sequences, the RF amplitudes of CT selective pulses were equal to 7 kHz on both ^{11}B and ^{27}Al quadrupolar channels, corresponding nutation frequencies of the CT equal to 14 kHz and 21 kHz, respectively. For all simulations, B_0 was equal to 9.4 T, and ν_R = 13.986 kHz. The quadrupolar parameters of ^{11}B and ^{27}Al were C_Q = 2 MHz and 3 MHz with η_Q = 0, respectively, expect in Figs. 3c,d, 4c,d, 6b,d and 8b,d, where the C_Q value was varied. The quadrupolar interactions of both isotopes were considered up to the second order. The ^{11}B-^{27}Al internuclear vector was aligned with the Z axes of the electric field gradient tensor of both nuclei, and the chemical shift anisotropies of both nuclei were null. The ^{11}B-^{27}Al dipolar coupling constant was fixed to $|b_{IS}/(2\pi)|$ = 370 Hz corresponding to an usual ^{11}B-^{27}Al distance of 300 pm. We simulated the transfer efficiency of both *D*-HMQC and *D*-RINEPT sequences. The rf pulses on both channels were applied on resonance, except in Figs. 3a,b, 4a,b, 6a,c and 8a,c. The simulated transfer efficiencies of *D*-HMQC and *D*-RINEPT sequences were normalized to the intensity of CT of the *S* spin measured after a CT-selective $\pi/2$ pulse. Note that Simpson software does not account for the Boltzmann distribution of the populations of the different energy levels, hence for signal enhancement equal to γ_I/γ_S, where γ_I and γ_S are the gyromagnetic ratios of the *I* and *S* spins, in the case of a magnetization transfer from *I* to *S* isotope, like in *S*{*I*} *D*-RINEPT sequence.

2.3 NMR measurements

Solid-state NMR experiments were carried out on glass samples with molar

composition 40%MgO-50%B_2O_3-10%Al_2O_3 prepared by melt-quenching procedure. A mixture of reagent grade magnesium carbonate, aluminum hydroxide and boric acid was melted at 1300 °C during 20 min before being quenched. This type of glass was proposed as a sealing glass.[61] The NMR experiments were recorded at 9.4 T on 400 MHz Bruker NMR spectrometer equipped with a 4 mm triple-channel HXY probe, for which ^{1}H, ^{11}B and ^{27}Al Larmor frequencies are equal to 400.1,128.3 and 104.3 MHz, respectively. The MAS frequency was equal to 13.986 kHz. Quantitative 1D ^{11}B and ^{27}Al NMR spectra were acquired by averaging 1024 transients with a recovery delay of 1 s using single-pulse NMR experiments with a pulse length of 0.78 and 0.62 μs, respectively, and an rf field strength of 50 and 40 kHz corresponding to a short tilt angle. For ^{11}B{^{27}Al} and ^{27}Al{^{11}B} *D*-HMQC and *D*-RINEPT experiments, the $C2_2^1$ recoupling scheme was applied on either ^{11}B or ^{27}Al channels, as shown in Figs. 1 and 2. The CT polarization of *S* spins was enhanced using QFS scheme. Typically, a sweep of 14 kHz was applied at offsets of the order of 90 to 200 kHz, depending on the scheme, during 400 μs to 4 ms and power ranging from 12 kHz to 32 kHz depending on scheme and pulse length. The CT selective π/2 and π pulses applied to ^{11}B and ^{27}Al nuclei lasted $\tau_{\pi/2,11B} = \tau_{\pi,11B}/2 = 11$ μs and $\tau_{\pi/2,27Al} = \tau_{\pi,27Al}/2 = 14$ μs, respectively. The τ_1 and τ_2 delays are indicated in the figure captions. The number of transients and t_1 increments as well as the recovery delay for the 2D ^{11}B{^{27}Al} and ^{27}Al {^{11}B} *D*-HMQC and *D*-RINEPT experiments are indicated in Table S1. ^{11}B and ^{27}Al NMR shift are referenced to $NaBH_4$ solid ($\delta_{iso} = -42.05$ ppm) and an 1 M solution of $Al(NO_3)_3$ ($\delta_{iso} = 0$ ppm), respectively.

3. Results and discussions

3.1 Numerical simulations

3.1.1 ^{11}B-^{27}Al *D*-HMQC

Direct observation on ^{11}B

We first investigate the case that ^{11}B nucleus is directly observed in ^{11}B {^{27}Al} *D*-HMQC experiments. According to the pulse sequence in Fig. 1, the recoupling pulse $C2_2^1$ could be employed on either observed spin channel (^{11}B, D^S-HMQC, Fig. 1a) or

indirect spin channel (^{27}Al, D^I-HMQC, Fig. 1b). Therefore, for an isolated spin pair ^{11}B-^{27}Al, only the quadrupolar spin irradiated by the dipolar recoupling pulses will be taken into account in next simulations. Fig. 3 clearly indicates that the D^I-HMQC scheme yields a higher maximal transfer efficiency (ca. 16%) than D^S-HMQC scheme (for which the maximal transfer efficiency does not exceed 12%). The ^{11}B{^{27}Al} D^I-HMQC sequence is more sensitive to offset than the D^S-HMQC scheme (compare Figs. 3a,b). The maximal transfer efficiency is achieved for C_Q = 3 MHz for both ^{11}B{^{27}Al} D^S- and D^I-HMQC experiments (see Figs. 3c,d). Finally ^{11}B{^{27}Al} D^I-HMQC experiments is more robust to rf field inhomogeneity than its D^S-HMQC counterpart, as shown in Figs. 3e,f.

Direct observation on ^{27}Al

In order to investigate the effect of the spin quantum number (spin-3/2 and spin-5/2) of irradiated nucleus to the polarization transfer efficiency in D^S- and D^I-HMQC schemes, we perform numerical simulations on ^{27}Al {^{11}B} *D*-HMQC experiments as well, in which the ^{27}Al spin is directly observed. In that case, D^I-HMQC variant again provides the highest maximal transfer efficiency: 24%, instead of 18% for D^S-HMQC variant. Furthermore, D^S-HMQC sequence is again more robust to the RF offset (Figs. 4a and b) as well as quadrupolar broadening of the irradiated quadrupolar spin (Figs. 4c and d) than the D^I-HMQC sequence. For ^{27}Al observation, D^I-HMQC technique benefits from higher robustness to rf inhomogeneity than D^S-HMQC method, like for ^{11}B observation (see Figs. 4e and f). Therefore, these simulation results suggest that the spin quantum number of quadrupolar spins has no essential influence on the performance of D^S- and D^I-HMQC schemes.

3.1.2 ^{11}B-^{27}Al *D*-RINEPT

Direct observation on ^{11}B

In a first step, we simulated the transfer efficiency of the four variants of ^{11}B{^{27}Al} *D*-RINEPT sequence shown in Fig. 2 as function of τ_1 (defocusing) and τ_2 (refocusing) periods (see Fig. 5). These simulations indicate that maximal transfer efficiency is

achieved for $\tau_1 = \tau_2 = 2.6$ and 1.3 ms for *II* and *SS* variants (see Figs. 5a and d), respectively, whereas the optimal τ_1 and τ_2 delays differ for *IS* and *SI* variants of ^{11}B{^{27}Al} *D*-RINEPT sequence. The D^{SS}-RINEPT scheme yields the highest ^{27}Al→^{11}B transfer efficiency (ca. 9%). The robustness of ^{11}B{^{27}Al} *D*-RINEPT sequences to rf offset and C_Q values has also been assessed using optimal τ_1 and τ_2 values (Fig. 6).

It easily finds that the RF offsets from both ^{11}B and ^{27}Al channels should have apparent influences on the transfer efficiencies of *SI* and *IS* variants. While *SI* variant scheme (Fig. 6c) seems to be less sensitive to the RF offset of ^{27}Al channel on which the recoupling pulses irradiate during refocusing period, and also have a better performance on the maximal transfer efficiency than *II* and *IS* variants. The optimal $C_Q(^{11}B)$ value is approximately equal to 3 MHz for the three *SS*, *IS* and *SI* variants, whereas the optimal $C_Q(^{27}Al)$ value is equal to 5.5 MHz for the *IS* and *II* variants. Similar to above *D*-HMQC simulations, the smaller and larger Cq values will be detrimental to the dipolar recoupling between two half-integer quadrupolar spins (Figs. 6b and d).

Direct observation on ^{27}Al

Similar simulations were performed for ^{27}Al {^{11}B} D-RINEPT experiments by using above four variants as well. As shown in Fig. 7, the best ^{11}B→^{27}Al transfer efficiency (ca. 13%) can be achieved by using the D^{II}-RINEPT scheme, which is seemingly contrary to above ^{11}B {^{27}Al} *D*-RINEPT results, in which the *SS* variant yields the highest maximal efficiency. Notably, both ^{27}Al {^{11}B} D^{II}-RINEPT and ^{11}B {^{27}Al} D^{SS}-RINEPT schemes apply the recoupling pulses to the same isotope channel (^{11}B), thus it probably suggests that recoupling on spin-3/2 should be more efficient than recoupling on spin-5/2 (^{27}Al) in ^{11}B-^{27}Al *D*-RINEPT measurements when ignoring effects of relaxations (T_1 and T_2). This can be further evidenced by the simulation results of ^{23}Na {^{11}B} *D*-RINEPT on an isolated ^{11}B-^{23}Na (two spin-3/2) spin pair, and no apparent difference is observed between *II* and *SS* variants (Fig. S1).

Interestingly, apart from the *SS* variant, the *SI* variant still has a better performance than *II* and *IS* variants (Fig.7 and Fig. 8), although the isotope channels irradiated by

recoupling pulses in ^{27}Al {^{11}B} D^{SI}-RINEPT are completely reversed with respect to ^{11}B {^{27}Al} D^{SI}-RINEPT.

3. 2 NMR experiments

Since it is difficult to find a sample with isolated ^{11}B-^{27}Al spin pairs, the glass sample 40%MgO/ 50%B_2O_3/ 10%Al_2O_3 is used to assess the overall performance of *D*-HMQC and *D*-RINEPT experiment with different recoupling channels. There are two kind of boron sites (B_{III} and B_{IV}, Fig. 9a) and three kind of aluminum sites (Al_{IV}, A_V and Al_{VI}, Fig. 9b) in the sample, whose NMR parameters deduced by 2D ^{11}B and ^{27}Al MQMAS experiments (not shown) as well as corresponding T_1 and T_2 values are listed in Table 1.

Usually the theoretical sensitivity (S/N) of heteronuclear correlation experiments between two half-integer quadrupolar isotopes can be expressed as follow by ignoring the transverse relaxation of the spin and the efficiency of the dipolar recoupling (assume keeping the same t_1 points),[62-64]

$$\frac{S}{N\sqrt{T_{tot}}} = \gamma_{exc}\gamma_{det}^{3/2}\varepsilon_{PT}\left(\frac{1}{2FWHM_{det}}\right)^{1/2}\frac{\left[1-exp\left(\frac{-\tau_{RD}}{T_1}\right)\right]}{\sqrt{\tau_{RD}}}$$

Where, T_{tot} is the total experimental time, γ_{exc} and γ_{det} are the gyromagnetic ratios of the initially excited nucleus and the directly observed nucleus, respectively. ε_{PT} is the enhancement factor of the initial CT signal of excited nucleus by saturating/inversing its satellite transitions, $FWHM_{det}$ represents the linewidth at half maximum of the directly observed resonances, and τ_{RD} is the relaxation delay used in the experiment. Therefore, Table 2 provides the relative NMR sensitivities of ^{11}B-^{27}Al HMQC/RINEPT experiments with the consideration of the experimental parameters in our measurements. For the glass sample, it clearly shows that the ^{11}B {^{27}Al} RINEPT experiment can obtain the maximal theoretical sensitivity due to the shorter T_1 of ^{27}Al, higher Larmor frequency and narrower FWHM of ^{11}B resonances.

Experimentally, the fast transverse relaxations (T_2) of ^{11}B (< 22 ms) and ^{27}Al (ca. 50 ms) species must be taken into account for the choice of recoupling channels, which should seriously impact the polarization transfer efficiency between ^{11}B and ^{27}Al as

well.

3.2.1 *D*-HMQC experiment

As shown in Fig. 10, the 1D *D*-HMQC build-up curves unambiguously illustrate that the D^I-HMQC scheme could achieve significantly higher maximal efficiency (ca. a factor of 4) than that of D^S-HMQC scheme, no matter it is the ^{11}B {^{27}Al } or ^{27}Al {^{11}B } HETCOR experiment, which seems beyond the expectation of the simulations in Section 3.1.1. Actually, there are many parameters that can affect the maximal transfer efficiencies between ^{11}B and ^{27}Al in the glass sample, including different quadrupolar interactions, RF offsets with respect to different sites, inaccurate selective $\pi/2$ and π pulse lengths as well as the dipolar network in the multiple-spin system. Note that, the R3 variant used here should also reintroduce chemical shift anisotropy (CSA) and homonuclear interactions of irradiated spins,[47-48] particularly the latter cannot be refocused by the middle π pulse in an echo-like experiment. In the investigated glass samples the homonuclear interactions can be significant, therefore such homonuclear interactions could result in a much faster dephasing of the CT magnetizations of observed spins on the transverse (X-Y) plane (see simulations in Fig. 2S), which are thus responsible for the marked attenuation of NMR signals from ^{11}B-^{27}Al polarization transfer in D^S-HMQC scheme. While in D^I-HMQC scheme the spin magnetizations (operators) of irradiated spins pointing towards the B_0 axis (along Z axis) does not commute with CAS and homonuclear interactions Hamiltonian. These could also explain such a big difference in the experimental efficiency between D^S- and D^I-HMQC schemes (Fig. 11c and Fig. 11f), compared to simulation results.

The 2D ^{11}B-^{27}Al HETCOR spectra acquired by using ^{11}B {^{27}Al} and ^{27}Al {^{11}B} *D*-HMQC with different recoupling channels (Fig. 1) are also displayed in Fig. 11. It shows that the three aluminum sites are all in close proximities with the three-coordinated boron site in the glass samples, however the severely overlapping of the lineshapes of two ^{11}B resonances makes it difficult to identify the existence of the affinity between tetrahedral boron site and aluminum sites. Indeed, the ^{11}B observed D^I-HMQC scheme can achieve the best sensitivity in the four 2D spectra, however,

there is an obvious artifact (ca. -40 ppm in Fig.7b) observed in F1 (^{27}Al) dimension, which might be ascribed to the t_1 noise originated from the insufficient relaxation recovery of ^{11}B CT magnetizations before each scan.[65] Meanwhile, the *D*-HMQC could yield somehow distortion of quadrupolar lineshape of indirectly observed spins owing to its multiple-quantum coherence evolving during t_1 period.

3.2.2 *D*-RINEPT experiment

Since the implementation of recoupling pulses can be divided into defocusing and refocusing parts (τ_1 and τ_2 in Fig. 2) in the D-RINEPT sequence, we explore the experimental buildup curves versus τ_1 and τ_2, respectively. Interestingly, the optimal recoupling times (τ_1 and τ_2) for defocusing and refocusing are not the same in D^{II}- and D^{SS}-RINEPT experiments (Fig. 12 and Fig. 13). This could be attributed to distinct orientations of the CT magnetization of the irradiated spin evolving during defocusing ($I_{x\text{-}y}$ and S_z) and refocusing (I_z and $S_{x\text{-}y}$) periods, thus one of recoupling periods will suffer from the effect of transverse relaxation decay. Despite simulations (section 3.1.2) suggest that applying the recoupling pulses to ^{11}B (spin-3/2) could achieve higher polarization transfer efficiency than applying it to ^{27}Al, experimental results in Fig. 12 (*SS* variant) and Fig. 13 (*II* variant) demonstrated the short T_2 of ^{11}B species (Table 1) critically affects the practical polarization transfer efficiency in ^{11}B-^{27}Al *D*-RINEPT experiments. It should emphasize that in D^{SI}-RINEPT scheme the recoupling pulses always irradiate on the nuclear spins whose CT magnetizations are along Z axis, thus the *SI* variant can obtain a better maximal signal compared to other three variant (also see Fig. 14d and Fig. 15d). On the contrary, D^{IS}-RINEPT scheme exhibits the worst efficiency, in which nuclear spins irradiated by the recoupling pulses evolve in the X-Y plane during both excitation and refocusing periods. The 2D ^{11}B-^{27}Al *D*-RINEPT spectra obtained by using different recoupling pathways are displayed in Fig. 14 and Fig. 15. Because single quantum coherence evolves during t_1 period, *D*-RINEPT experiment can alleviate the influence of t_1 noise compared to *D*-HMQC experiment. In addition, it can be found that the quadrupolar lineshape of three-coordinated ^{11}B signal was well preserved in indirect dimension in ^{27}Al {^{11}B} D-RINEPT experiments

(Fig. 15a-c). As shown in Fig. 16, ^{11}B{^{27}Al} D^{I}-HMQC scheme seems to exhibit a higher sensitivity than ^{11}B{^{27}Al} D^{S}-RINEPT scheme, however, the total acquisition time of the former is about four times that of the latter under the same number of scans. This is because the initial magnetizations in ^{11}B{^{27}Al} D-HMQC and D-RINEPT experiments come from ^{11}B spins and ^{27}Al spins, respectively, while ^{11}B has a much longer T_1 than ^{27}Al in the glass sample (Table 1). Therefore, it means the ^{11}B{^{27}Al} D^{SI}-RINEPT scheme actually have a better performance than ^{11}B{^{27}Al} D^{I}-HMQC scheme when keeping the same experimental times, which is also in agreement with the theoretical calculations in Table 2.

Conclusions

Despite a variety of NMR parameters can affect the practical polarization transfer efficiency between two half-integer quadrupolar hetero-nuclei in *D*-HMQC and *D*-RINEPT sequences, here we focus on a detailed study on the influence of recoupling channels selected in ^{11}B-^{27}Al HETCOR experiments by using above sequences. Both simulations and experiments suggest that employing the dipolar recoupling pulses on the indirectly observed spin channel (no matter spin-3/2 or spin-5/2) rather than directly observed spin channel could achieve efficient polarization transfer between ^{11}B and ^{27}Al in *D*-HMQC measurements, where the indirectly observed spin does not evolved on the X-Y plane during recoupling periods (Fig. 1b). Although simulations show the recoupling pulses that always irradiate on the spin-3/2 (^{11}B) channel can obtain a higher sensitivity in both ^{11}B {^{27}Al} and ^{27}Al {^{11}B} *D*-RINEPT measurements, experimental results clearly indicate that applying the recoupling pulses to the spin channel where the magnetization does not dephase (along Z axis) will help to maintain the polarization coherence, that is recoupling on observed channel *S* during excitation and on indirectly observed channel *I* during refocusing (Fig. 2d). Hence, it means the transverse dephasing of the spin evolving on the X-Y plane plays a leading role to the practical transfer efficiency in both ^{11}B-^{27}Al *D*-HMQC and *D*-RINEPT measurements. In addition to the recoupling pathways, the longitudinal relaxation (T_1) of the initial polarized spin as well as the absolute sensitivity of directly observed spins should be

also taken into account for the selection of pulse sequences in practical applications of such ^{11}B-^{27}Al HETCOR experiments. Conclusively, we believe the in-depth understanding of the *D*-HMQC and *D*-RINEPT sequence allow to a better implementation of such HETCOR experiments between two half-integer quadrupolar hetero-nuclei, which should become very useful and provide detailed insight to the structure and properties of many relevant materials.

Acknowledgement

This work was supported by the National Natural Science Foundation of China (Grants, 91745111, 21622311, U1932218, 21733013 and 21872170), key program for frontier science of the Chinese Academy of Sciences (QYZDB-SSW-SLH027), Hubei Provincial Natural Science Foundation (2017CFA032), and Youth Innovation Promotion Association, Chinese Academy of Sciences. Dr. Gregory Tricot (Univ. Lille, LASIRE) is acknowledged for providing the investigated glass sample. Chevreul institute (FR 2638), Ministère de l'Enseignement Supérieur, de la Recherche et de l'Innovation, Hauts-de-France Region and FEDER are acknowledged for supporting and funding partially this work. Financial support from the IR-RMN-THC FR-3050 CNRS for conducting the research is gratefully acknowledged. Authors also thank contract ANR-18-CE08-0015-01 (ThinGlass). This project has received funding from the European Union's Horizon 2020 research and innovation program under grant agreement No 731019 (EUSMI). OL acknowledge financial support from Institut Universitaire de France (IUF).

Reference

1. van Bokhoven, J. A.; Koningsberger, D. C.; Kunkeler, P.; van Bekkum, H.; Kentgens, A. P. M., Stepwise dealumination of zeolite beta at specific T-sites observed with Al-27 MAS and Al-27 MQ MAS NMR. *J Am Chem Soc* **2000,** *122* (51), 12842-12847.
2. Fyfe, C. A.; Feng, Y.; Grondey, H.; Kokotailo, G. T.; Gies, H., One-dimensional and 2-dimensional high-resolution solid-state nmr-studies of zeolite lattice structures. *Chem Rev* **1991,** *91* (7), 1525-1543.
3. Rowles, M. R.; Hanna, J. V.; Pike, K. J.; Smith, M. E.; O'Connor, B. H., Si-29, Al-27, H-1 and Na-23 MAS NMR study of the bonding character in aluminosilicate inorganic polymers. *Appl Magn*

Reson **2007,** *32* (4), 663-689.
4. Gervais, C.; Maquet, J.; Babonneau, F.; Duriez, C.; Framery, E.; Vaultier, M.; Florian, P.; Massiot, D., Chemically derived BN ceramics: Extensive B-11 and N-15 solid-state NMR study of a preceramic polyborazilene. *Chem Mater* **2001,** *13* (5), 1700-1707.
5. Harris, R. K.; Leach, M. J.; Thompson, D. P., N-15 AND O-17 NMR-SPECTROSCOPY OF SILICATES AND NITROGEN CERAMICS. *Chem Mater* **1992,** *4* (2), 260-267.
6. O'Dell, L. A.; Rossini, A. J.; Schurko, R. W., Acquisition of ultra-wideline NMR spectra from quadrupolar nuclei by frequency stepped WURST-QCPMG. *Chem Phys Lett* **2009,** *468* (4-6), 330-335.
7. Kroeker, S.; Stebbins, J. F., Three-coordinated boron-11 chemical shifts in borates. *Inorg Chem* **2001,** *40* (24), 6239-6246.
8. Laurencin, D.; Gervais, C.; Wong, A.; Coelho, C.; Mauri, F.; Massiot, D.; Smith, M. E.; Bonhomme, C., Implementation of High Resolution Ca-43 Solid State NMR Spectroscopy: Toward the Elucidation of Calcium Sites in Biological Materials. *J Am Chem Soc* **2009,** *131* (37), 13430-13440.
9. Rovnyak, D.; Baldus, M.; Wu, G.; Hud, N. V.; Feigon, J.; Griffin, R. G., Localization of Na-23(+) in a DNA quadruplex by high-field solid-state NMR. *J Am Chem Soc* **2000,** *122* (46), 11423-11429.
10. Perras, F. A.; Viger-Gravel, J.; Burgess, K. M. N.; Bryce, D. L., Signal enhancement in solid-state NMR of quadrupolar nuclei. *Solid State Nucl Mag* **2013,** *51-52*, 1-15.
11. Ashbrook, S. E., Recent advances in solid-state NMR spectroscopy of quadrupolar nuclei. *Phys Chem Chem Phys* **2009,** *11* (32), 6892-6905.
12. Trebosc, J.; Hu, B.; Amoureux, J. P.; Gan, Z., Through-space R-3-HETCOR experiments between spin-1/2 and half-integer quadrupolar nuclei in solid-state NMR. *J Magn Reson* **2007,** *186* (2), 220-227.
13. Wang, Q.; Hu, B.; Lafon, O.; Trebosc, J.; Deng, F.; Amoureux, J. P., Double-quantum homonuclear NMR correlation spectroscopy of quadrupolar nuclei subjected to magic-angle spinning and high magnetic field. *J Magn Reson* **2009,** *200* (2), 251-260.
14. Smith, M. E.; van Eck, E. R. H., Recent advances in experimental solid state NMR methodology for half-integer spin quadrupolar nuclei. *Prog Nucl Mag Res Sp* **1999,** *34* (2), 159-201.
15. Medek, A.; Harwood, J. S.; Frydman, L., Multiple-quantum magic-angle spinning NMR: A new method for the study of quadrupolar nuclei in solids. *J Am Chem Soc* **1995,** *117* (51), 12779-12787.
16. Kentgens, A. P. M., A practical guide to solid-state NMR of half-integer quadrupolar nuclei with some applications to disordered systems. *Geoderma* **1997,** *80* (3-4), 271-306.
17. Ashbrook, S. E.; Smith, M. E., Solid state O-17 NMR - an introduction to the background principles and applications to inorganic materials. *Chem Soc Rev* **2006,** *35* (8), 718-735.
18. Qi, G. D.; Wang, Q.; Xu, J.; Trebosc, J.; Lafon, O.; Wang, C.; Amoureux, J. P.; Deng, F., Synergic Effect of Active Sites in Zinc-Modified ZSM-5 Zeolites as Revealed by High-Field Solid-State NMR Spectroscopy. *Angew Chem Int Edit* **2016,** *55* (51), 15826-15830.
19. Wang, C.; Wang, Q.; Xu, J.; Qi, G. D.; Gao, P.; Wang, W. Y.; Zou, Y. Y.; Feng, N. D.; Liu, X. L.; Deng, F., Direct Detection of Supramolecular Reaction Centers in the Methanolto- Olefins Conversion over Zeolite H-ZSM-5 by C-13-Al-27 Solid-State NMR Spectroscopy. *Angew Chem Int Edit* **2016,** *55* (7), 2507-2511.
20. Yu, Z. W.; Zheng, A. M.; Wang, Q. A.; Chen, L.; Xu, J.; Amoureux, J. P.; Deng, F., Insights into the Dealumination of Zeolite HY Revealed by Sensitivity-Enhanced Al-27 DQ-MAS NMR Spectroscopy at High Field. *Angew Chem Int Edit* **2010,** *49* (46), 8657-8661.
21. Haouas, M.; Taulelle, F.; Martineau, C., Recent advances in application of Al-27 NMR

spectroscopy to materials science. *Prog Nucl Mag Res Sp* **2016,** *94-95*, 11-36.
22. Ashbrook, S. E.; Griffin, J. M.; Johnston, K. E., Recent Advances in Solid-State Nuclear Magnetic Resonance Spectroscopy. In *Annual Review Of Analytical Chemistry, Vol 11*, Bohn, P. W.; Pemberton, J. E., Eds. Annual Reviews: Palo Alto, 2018; Vol. 11, pp 485-508.
23. Bonhomme, C.; Gervais, C.; Laurencin, D., Recent NMR developments applied to organic-inorganic materials. *Prog Nucl Mag Res Sp* **2014,** *77*, 1-48.
24. van Wüllen, L.; Züchner, L.; Müller-Warmuth, W.; Eckert, H., 11B{27Al} and Al{11B} double resonance experiments on a glassy sodium aluminoborate. *Solid State Nucl Mag* **1996,** *6* (3), 203-212.
25. Chan, J. C. C.; Bertmer, M.; Eckert, H., Double-quantum cross-polarization between half-integer quadrupolar spin systems: 11B↔23Na and 11B↔27Al. *Chem Phys Lett* **1998,** *292* (1), 154-160.
26. Chan, J. C. C.; Bertmer, M.; Eckert, H., Site Connectivities in Amorphous Materials Studied by Double-Resonance NMR of Quadrupolar Nuclei: High-Resolution 11B ↔ 27Al Spectroscopy of Aluminoborate Glasses. *J Am Chem Soc* **1999,** *121* (22), 5238-5248.
27. Lu, X.; Tankamony, A. S. L.; Trébosc, J.; Lafon, O.; Amoureux, J.-P., Probing proximities between different quadrupolar isotopes using multi-pulse cross-polarization. *J Magn Reson* **2013,** *228*, 148-158.
28. Fernandez, C.; Morais, C.; Rocha, J.; Pruski, M., High-resolution heteronuclear correlation spectra between P-31 and Al-27 in microporous aluminophosphates. *Solid State Nucl Mag* **2002,** *21* (1-2), 61-70.
29. Vega, A. J., MAS NMR spin locking of half-integer quadrupolar nuclei. *J Magn Reson* **1992,** *96* (1), 50-68.
30. Vega, A. J., CP/MAS of quadrupolar S=3/2 nuclei. *Solid State Nucl Mag* **1992,** *1* (1), 17-32.
31. Amoureux, J. P.; Pruski, M., Theoretical and experimental assessment of single- and multiple-quantum cross-polarization in solid state NMR. *Mol Phys* **2002,** *100* (10), 1595-1613.
32. Xin, S. H.; Wang, Q.; Xu, J.; Feng, N. D.; Li, W. Z.; Deng, F., Heteronuclear correlation experiments of Na-23-Al-27 in rotating solids. *Solid State Nucl Mag* **2017,** *84*, 103-110.
33. Duong, N. T.; Nishiyama, Y., Satellite and central transitions selective H-1/{Al-27} D-HMQC experiments at very fast MAS for quadrupolar couplings determination. *Solid State Nucl Mag* **2017,** *84*, 83-88.
34. Wang, Q.; Li, Y.; Trebosc, J.; Lafon, O.; Xu, J.; Hu, B.; Feng, N.; Chen, Q.; Amoureux, J.-P.; Deng, F., Population transfer HMQC for half-integer quadrupolar nuclei. *J Chem Phys* **2015,** *142* (9).
35. Trebosc, J.; Lafon, O.; Hu, B. W.; Amoureux, J. P., Indirect high-resolution detection for quadrupolar spin-3/2 nuclei in dipolar HMQC solid-state NMR experiments. *Chem Phys Lett* **2010,** *496* (1-3), 201-207.
36. Lafon, O.; Wang, Q.; Hu, B.; Vasconcelos, F.; Trebosc, J.; Cristol, S.; Deng, F.; Amoureux, J.-P., Indirect Detection via Spin-1/2 Nuclei in Solid State NMR Spectroscopy: Application to the Observation of Proximities between Protons and Quadrupolar Nuclei. *J Phys Chem A* **2009,** *113* (46), 12864-12878.
37. Wijesekara, A. V.; Venkatesh, A.; Lampkin, B. J.; VanVeller, B.; Lubach, J. W.; Nagapudi, K.; Hung, I.; Gor'kov, P. L.; Gan, Z. H.; Rossini, A. J., Fast Acquisition of Proton-Detected HETCOR Solid-State NMR Spectra of Quadrupolar Nuclei and Rapid Measurement of NH Bond Lengths by Frequency Selective HMQC and RESPDOR Pulse Sequences. *Chem-eur J* **2020,** *26* (35), 7881-7888.
38. Venkatesh, A.; Hanrahan, M. P.; Rossini, A. J., Proton detection of MAS solid-state NMR spectra of half-integer quadrupolar nuclei. *Solid State Nucl Mag* **2017,** *84*, 171-181.

39. Amoureux, J. P.; Trebosc, J.; Wiench, J.; Pruski, M., HMQC and refocused-INEPT experiments involving half-integer quadrupolar nuclei in solids. *J Magn Reson* **2007,** *184* (1), 1-14.
40. Tokatli, A.; Gencten, A.; Sahin, M.; Tezel, O.; Bahceli, S., Product operator descriptions of INEPT and RINEPT NMR spectroscopies for ISn (I=1/2, S=3/2) spin systems. *J Magn Reson* **2004,** *169* (1), 68-72.
41. Kao, H. M.; Grey, G. P., INEPT experiments involving quadrupolar nuclei in solids. *J Magn Reson* **1998,** *133* (2), 313-323.
42. Fyfe, C. A.; Wongmoon, K. C.; Huang, Y.; Grondey, H., INEPT experiments in solid-state NMR. *J Am Chem Soc* **1995,** *117* (41), 10397-10398.
43. Altvater, N. R.; Dorn, R. W.; Cendejas, M. C.; McDermott, W. P.; Thomas, B.; Rossini, A. J.; Hermans, I., B-MWW Zeolite: The Case Against Single-Site Catalysis. *Angew Chem Int Edit* **2020,** *59* (16), 6546-6550.
44. Carnahan, S. L.; Lampkin, B. J.; Naik, P.; Hanrahan, M. P.; Slowing, II; VanVeller, B.; Wu, G.; Rossini, A. J., Probing O-H Bonding through Proton Detected H-1-O-17 Double Resonance Solid-State NMR Spectroscopy. *J Am Chem Soc* **2019,** *141* (1), 441-450.
45. Brinkmann, A.; Kentgens, A. P. M., Proton-selective O-17-H-1 distance measurements in fast magic-angle-spinning solid-state NMR spectroscopy for the determination of hydrogen bond lengths. *J Am Chem Soc* **2006,** *128* (46), 14758-14759.
46. Levitt, M. H., Symmetry-based pulse sequences in magic-angle spinning solid-state NMR. In *Encyclopedia of Nuclear Magnetic Resonance* Grant, D. M. H., R.K., Ed. John Wiley & Sons, Ltd, Chichester, UK: 2002.
47. Costa, P. R.; Gross, J. D.; Hong, M.; Griffin, R. G., Solid-state NMR measurement of Ψ in peptides: a NCCN 2Q-heteronuclear local field experiment. *Chem Phys Lett* **1997,** *280* (1), 95-103.
48. Levitt, M. H.; Oas, T. G.; Griffin, R. G., Rotary resonance recoupling in heteronuclear spin pair systems. *Israel J Chem* **1988,** *28* (4), 271-282.
49. Levitt, M. H., Symmetry in the design of NMR multiple-pulse sequences. *J Chem Phys* **2008,** *128* (5).
50. Iuga, D.; Schafer, H.; Verhagen, R.; Kentgens, A. P. M., Population and coherence transfer induced by double frequency sweeps in half-integer quadrupolar spin systems. *J Magn Reson* **2000,** *147* (2), 192-209.
51. Kentgens, A. P. M.; Verhagen, R., Advantages of double frequency sweeps in static, MAS and MQMAS NMR of spin I=3/2 nuclei. *Chem Phys Lett* **1999,** *300* (3-4), 435-443.
52. Siegel, R.; Nakashima, T. T.; Wasylishen, R. E., Sensitivity enhancement of NMR spectra of half-integer spin quadrupolar nuclei in solids using hyperbolic secant pulses. *J Magn Reson* **2007,** *184* (1), 85-100.
53. Siegel, R.; Nakashima, T. T.; Wasylishen, R. E., Signal enhancement of NMR spectra of half-integer quadrupolar nuclei in solids using hyperbolic secant pulses. *Chem Phys Lett* **2004,** *388* (4-6), 441-445.
54. Brauniger, T.; Hempel, G.; Madhu, P. K., Fast amplitude-modulated pulse trains with frequency sweep (SW-FAM) in static NMR of half-integer spin quadrupolar nuclei. *J Magn Reson* **2006,** *181* (1), 68-78.
55. Madhu, P. K.; Goldbourt, A.; Frydman, L.; Vega, S., Fast radio-frequency amplitude modulation in multiple-quantum magic-angle-spinning nuclear magnetic resonance: Theory and experiments. *J Chem Phys* **2000,** *112* (5), 2377-2391.

56. Yao, Z.; Kwak, H. T.; Sakellariou, D.; Emsley, L.; Grandinetti, P. J., Sensitivity enhancement of the central transition NMR signal of quadrupolar nuclei under magic-angle spinning. *Chem Phys Lett* **2000,** *327* (1-2), 85-90.
57. Wang, Q.; Trebosc, J.; Li, Y. X.; Lafon, O.; Xin, S. H.; Xu, J.; Hu, B. W.; Feng, N. D.; Amoureux, J. P.; Deng, F., Uniform signal enhancement in MAS NMR of half-integer quadrupolar nuclei using quadruple-frequency sweeps. *J Magn Reson* **2018,** *293*, 92-103.
58. Bak, M.; Rasmussen, J. T.; Nielsen, N. C., SIMPSON: A general simulation program for solid-state NMR spectroscopy. *J Magn Reson* **2000,** *147* (2), 296-330.
59. Conroy, H., MOLECULAR SCHRODINGER EQUATION .8. A NEW METHOD FOR EVALUATION OF MULTIDIMENSIONAL INTEGRALS. *J Chem Phys* **1967,** *47* (12), 5307-&.
60. Zaremba, S. K., Good lattice points, discrepancy, and numerical integration. *Annali di Matematica Pura ed Applicata* **1966,** *73* (1), 293-317.
61. Brow, R. K.; Tallant, D. R., Structural design of sealing glasses. *J Non-cryst Solids* **1997,** *222*, 396-406.
62. Althaus, S. M.; Mao, K. M.; Stringer, J. A.; Kobayashi, T.; Pruski, M., Indirectly detected heteronuclear correlation solid-state NMR spectroscopy of naturally abundant N-15 nuclei. *Solid State Nucl Mag* **2014,** *57-58*, 17-21.
63. Ishii, Y.; Tycko, R., Sensitivity enhancement in solid state N-15 NMR by indirect detection with high-speed magic angle spinning. *J Magn Reson* **2000,** *142* (1), 199-204.
64. Mao, K.; Wiench, J. W.; Lin, V. S. Y.; Pruski, M., Indirectly detected through-bond chemical shift correlation NMR spectroscopy in solids under fast MAS: Studies of organic-inorganic hybrid materials. *J Magn Reson* **2009,** *196* (1), 92-95.
65. Venkatesh, A.; Luan, X. C.; Perras, F. A.; Hung, I.; Huang, W. Y.; Rossini, A. J., t(1)-Noise eliminated dipolar heteronuclear multiple-quantum coherence solid-state NMR spectroscopy. *Phys Chem Chem Phys* **2020,** *22* (36), 20815-20828.

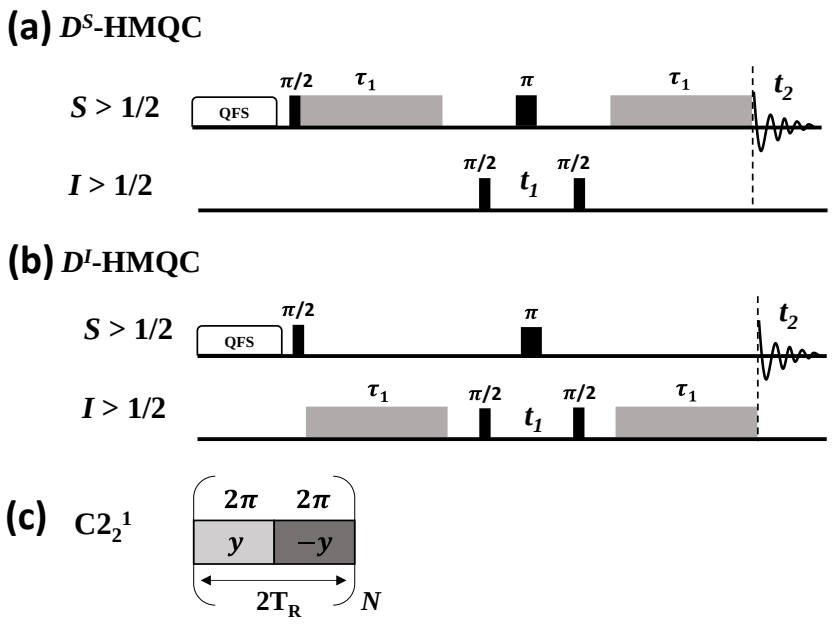

Figure 1. *(a) D^S- and (b) D^I-HMQC sequences, in which the polarization of CT of S spin is enhanced before the first π/2 pulse by the application of QFS scheme. The black solid squares represent the CT-selective π/2 and π pulses, while the heteronuclear dipolar recoupling blocks are displayed as grey rectangles. These recoupling blocks must be rotor-synchronized and we employed equal defocusing and refocusing periods $\tau_1 = 2NT_R$, where N is an integer and $T_R = 1/\nu_R$ is the rotor period. (c) The employed heteronuclear recoupling is based on $C2_2^1$ symmetry and consists of a train of CT-selective 2π pulses lasting T_R*

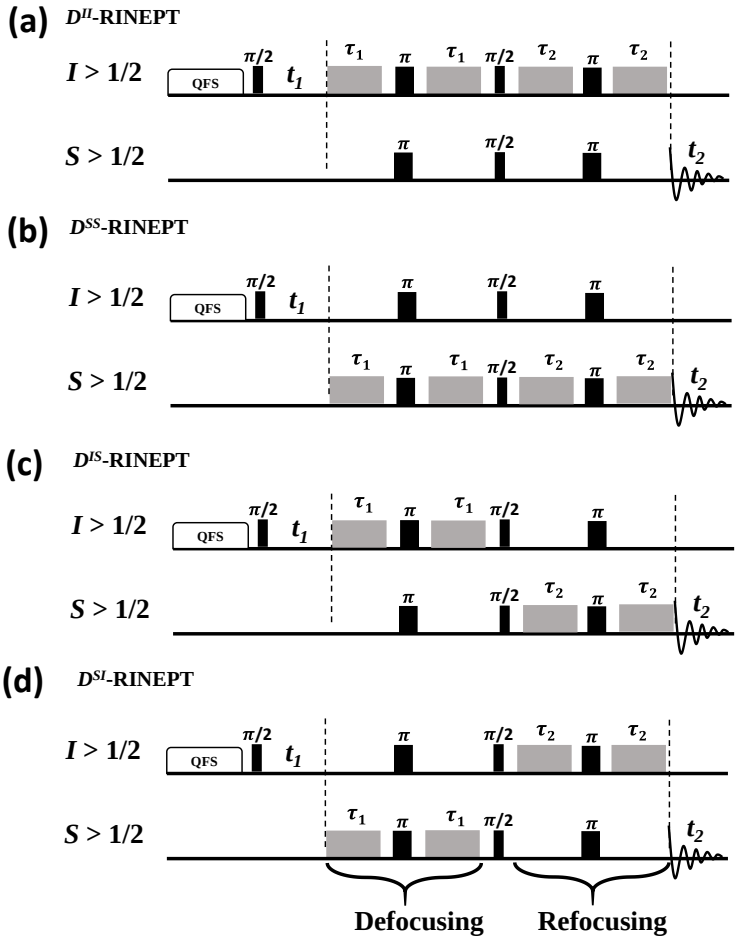

Figure 2. *(a) D^{II}-, (b) D^{SS}-, (c) D^{IS}- and (d) D^{SI}-RINEPT variants using defocusing and refocusing delays $\tau_1 = 2N_1T_R$ and $\tau_2 = 2N_2T_R$. The polarization of CT of I spin is enhanced before the first π/2 pulse by the application of QFS scheme. The black solid squares represent the CT-selective π/2 and π pulses, while the heteronuclear dipolar recoupling blocks are displayed as grey rectangles.*

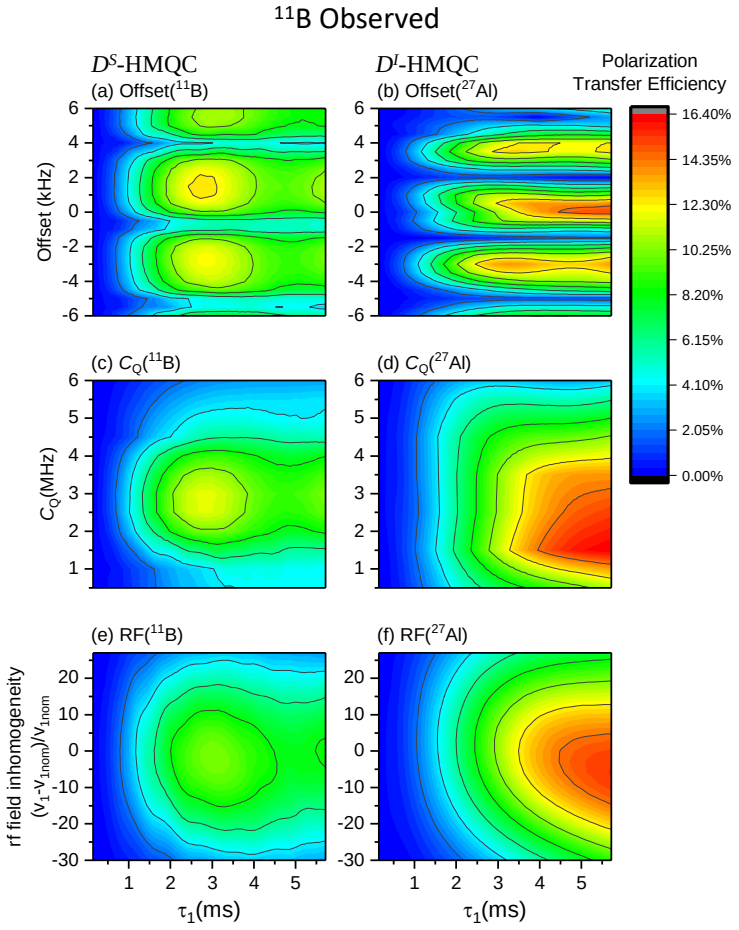

Figure 3. *Simulated transfer efficiency of $^{11}B\{^{27}Al\}$ (a,c,e) D^S- and (b,d,f) D^I-HMQC sequences as a function of τ_1 and (a, b) resonance offset and (c, d) C_Q value or (e, f) the deviation of the rf field of recoupling pulses from its nominal value, $(\nu_1 - \nu_{1nom})/\nu_{1nom}$ for the nucleus to which the recoupling is applied.*

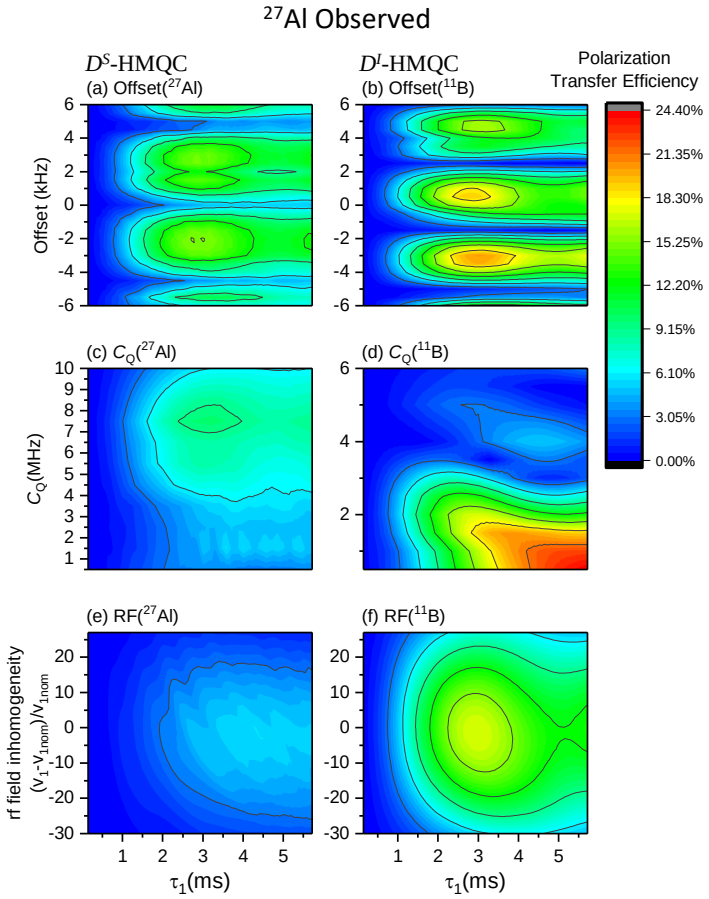

Figure 4. *Simulated transfer efficiency of ^{27}Al{^{11}B} (a,c,e) D^S- and (b,d,f) D^I-HMQC sequences as a function of τ_1 and (a, b) resonance offset and (c, d) C_Q value or (e, f) the deviation of the rf field of recoupling pulses from its nominal value, $(\nu_1-\nu_{1nom})/\nu_{1nom}$ for the nucleus to which the recoupling is applied.*

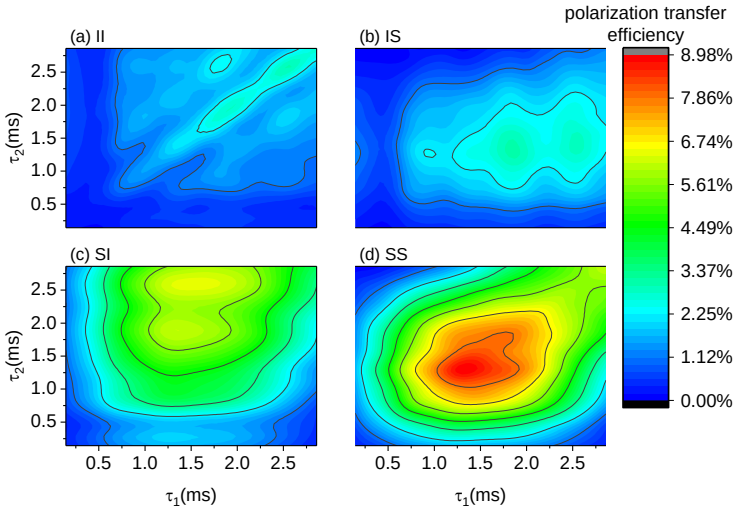

Figure 5. *Simulated $^{27}Al \rightarrow {}^{11}B$ transfer efficiencies of $^{11}B\{^{27}Al\}$ (a) D^{II}-, (b) D^{IS}-, (c) D^{SI}- and (d) D^{SS}-RINEPT sequences as a function of τ_1 and τ_2 delays.*

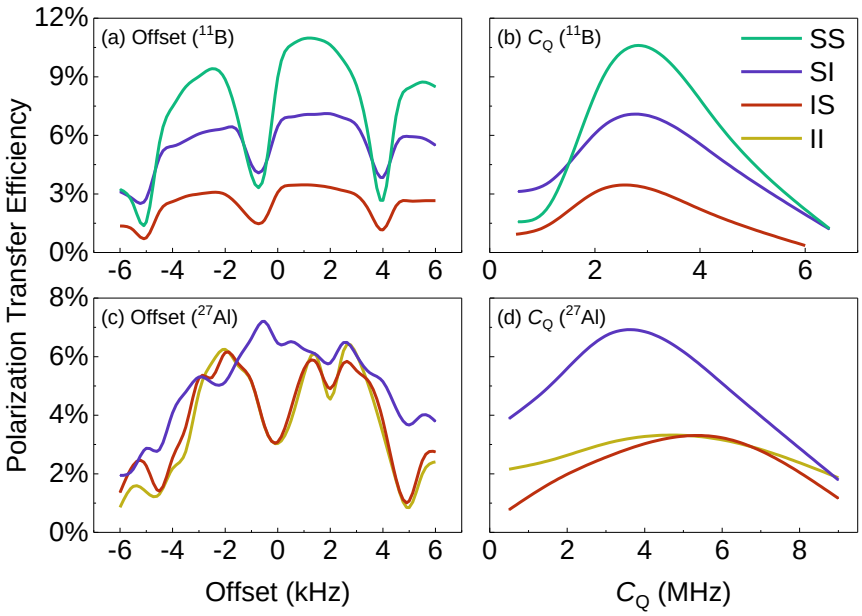

Figure 6. *Simulated transfer efficiencies of ^{11}B {^{27}Al} D^{II}- (yellow), D^{IS}- (red), D^{SI}- (purple) and D^{SS}(cyan)-RINEPT sequences as function of (a,c) resonance offset and (b,d) C_Q value of (a,b) ^{11}B and (c,d) ^{27}Al nuclei. The simulations were performed using optimal τ_1 and τ_2 delays determined from Fig. 5.*

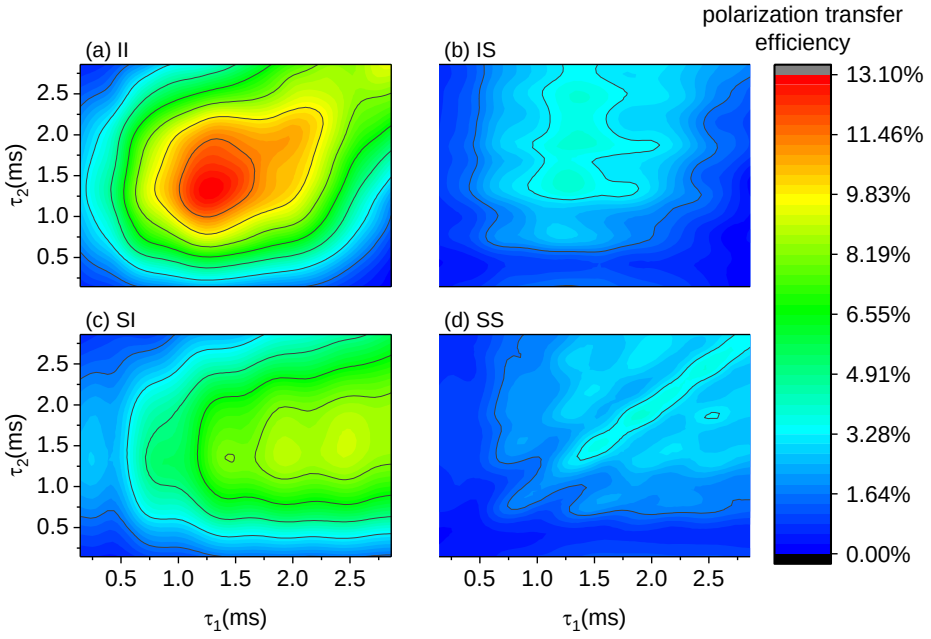

Figure 7. *Simulated $^{11}B \rightarrow ^{27}Al$ transfer efficiencies of ^{27}Al {^{11}B} (a) D^{II}-, (b) D^{IS}-, (c) D^{SI}- and (d) D^{SS}-RINEPT sequences as a function of τ_1 and τ_2 delays.*

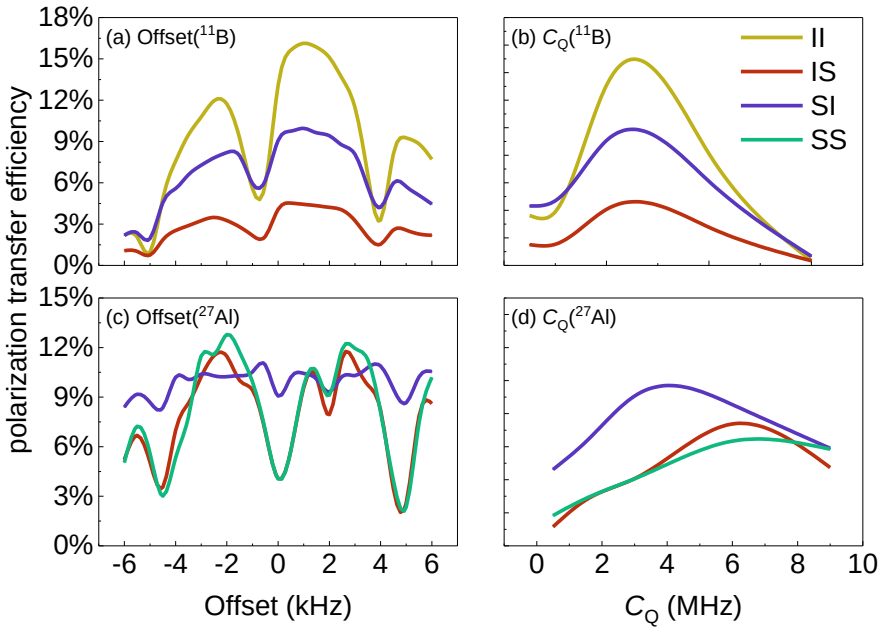

Figure 8. *Simulated transfer efficiencies of ^{27}Al {^{11}B} D^{II}- (yellow), D^{IS}- (red), D^{SI}- (purple) and D^{SS}(cyan)-RINEPT sequences as function of (a,c) resonance offset and (b,d) C_Q value of (a,b) ^{11}B and (c,d) ^{27}Al nuclei. The simulations were performed using optimal τ_1 and τ_2 delays determined from Fig. 2.*

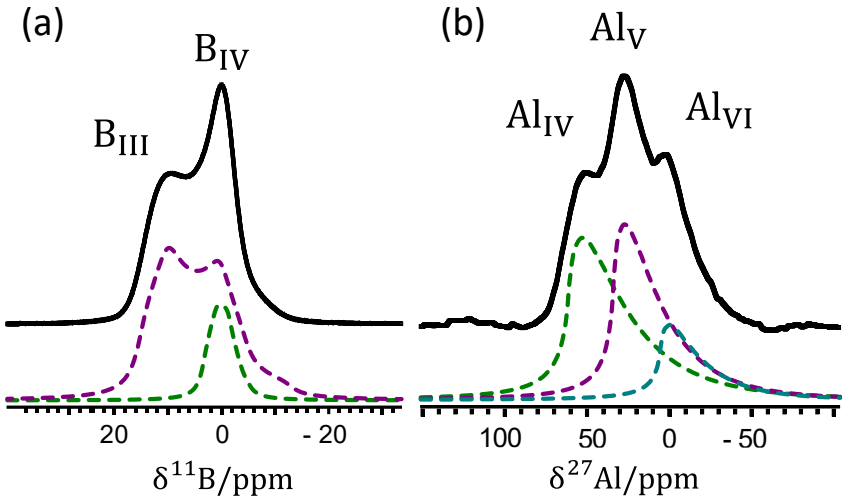

Figure 9. Peak fitting of ^{11}B (a) and ^{27}Al (b) MAS 1D spectra with a spinning speed at 10 kHz, small flip angle of $\pi/6$ (0.78μs for ^{11}B and 0.62μs for ^{27}Al) with a relaxation delay of 1s. The solid lines represent the experimental MAS 1D spectra. And the dashed lines represent the fitted peaks. The NMR parameters obtained by peak fitting are listed in Table 1.

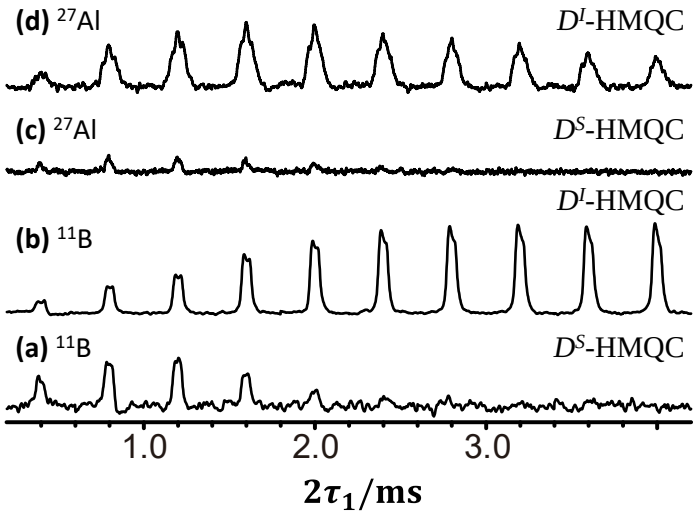

Figure 10. *Build-up curves of* $^{11}\mathrm{B} \rightarrow {}^{27}\mathrm{Al} \rightarrow {}^{11}\mathrm{B}$ *and* $^{27}\mathrm{Al} \rightarrow {}^{11}\mathrm{B} \rightarrow {}^{27}\mathrm{Al}$ *polarization transfer by using D-HMQC sequence in Fig. 1a and 1b, including* $^{11}B\ \{^{27}Al\}$ *D-HMQC spectra with recoupling pulses on* ^{11}B *channel (a) and* ^{27}Al *channel (b),* $^{27}Al\ \{^{11}B\}$ *D-HMQC spectra with recoupling pulses on* ^{27}Al *channel (c) and* ^{11}B *channel (d). 64, 64, 128 and 128 acquisitions are accumulated for (a), (b), (c) and (d), respectively.*

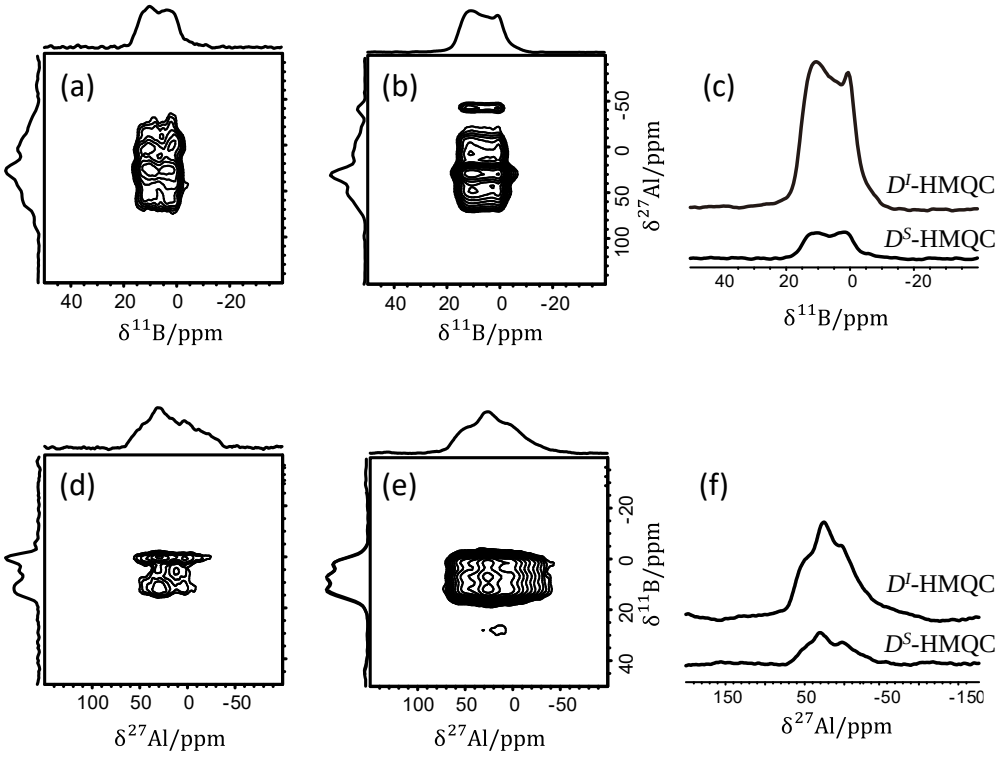

Figure 11. *2D ^{11}B-^{27}Al HETCOR spectra acquired using (a) ^{11}B{^{27}Al} D^S-HMQC, (b) ^{11}B{^{27}Al} D^I-HMQC, (d) ^{27}Al {^{11}B} D^S-HMQC and (e) ^{27}Al{^{11}B} D^I-HMQC sequences with τ_I = 0.8, 3.2, 0.8 and 1.6 ms, respectively. (c) Comparison of 1D ^{11}B skyline projection between 2D ^{11}B{^{27}Al} (bottom) D^S- and (top) D^I-HMQC spectra. (f) Comparison of 1D ^{27}Al skyline projection between 2D ^{27}Al{^{11}B} (bottom) D^S- and (top) D^I-HMQC spectra.*

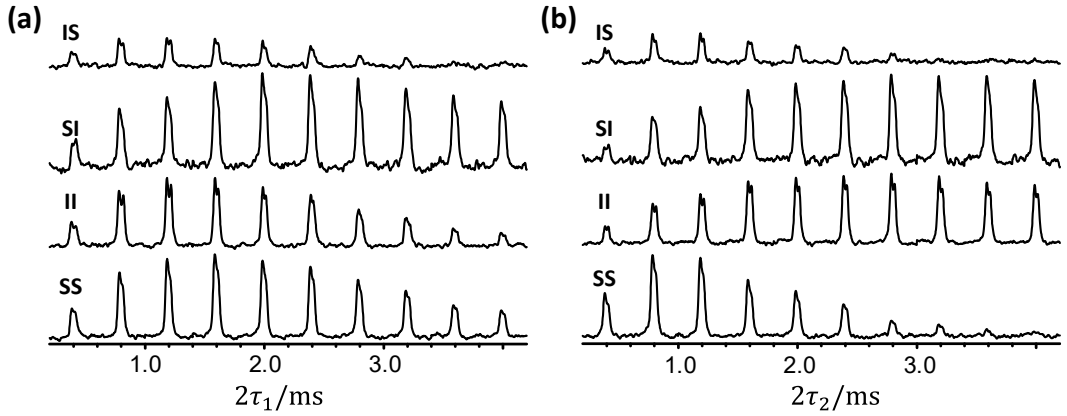

Figure 12. *Build-up curves of τ_1 (a) and τ_2 (b) by using four ^{11}B {^{27}Al} D-RINEPT schemes in* ***Fig. 2*** *(from top to bottom, IS, SI, II and SS). When optimizing τ_1, τ_2 are fixed at 1.2, 2.8, 2.8 and 0.8ms for IS, SI, II and SS variants, respectively. While τ_2 is fixed at 1.0, 2.0, 1.6 and 1.6ms for IS, SI, II and SS variants, respectively, when optimizing τ_2. 32 acquisitions are accumulated for the measurements of each 1D spectrum.*

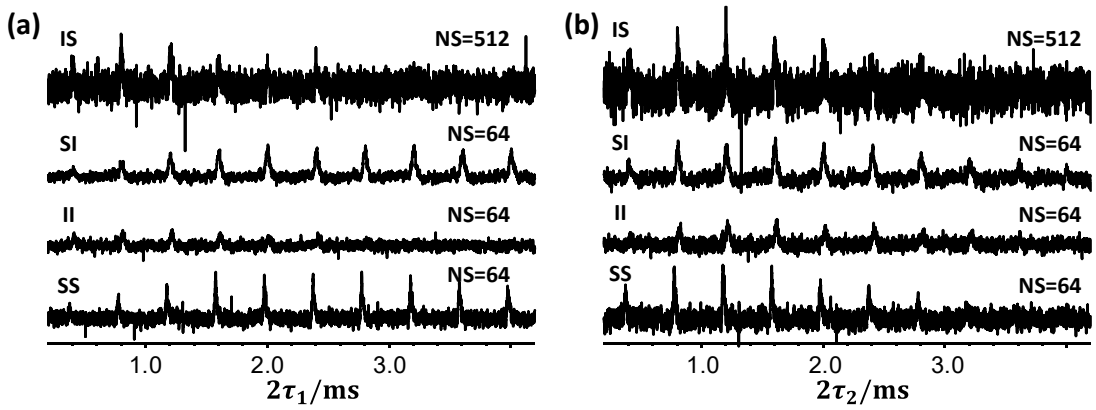

Figure 13. *Build-up curves of (a) τ_1 and (b) τ_2 delays by using four ^{27}Al {^{11}B} D-RINEPT schemes in* ***Fig. 2*** *(from top to bottom, IS, SI, II and SS). When optimizing τ_1, τ_2 are fixed at 1.2, 1.6, 1.6 and 1.2ms for IS, SI, II and SS variants, respectively. While τ_2 is fixed at 0.8, 2.0, 1.2 and 2.8ms for IS, SI, II and SS variants, respectively, when optimizing τ_2. NS represents number of scans used in the 1D measurement. Except for IS variant, 64 acquisitions are accumulated for the measurements of each 1D spectrum.*

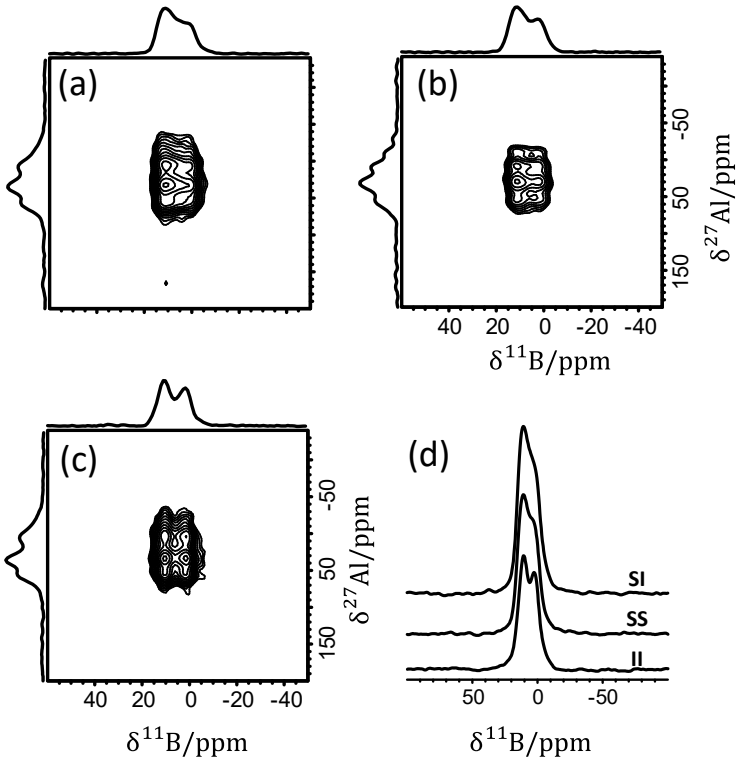

Figure 14. *2D ^{11}B-^{27}Al HETCOR spectra acquired using ^{11}B{^{27}Al} (a) D^{SI}-, (b) D^{SS}- and (c) D^{II}-RINEPT sequences with {τ_1, τ_2} = (2.0, 2.8), (1.6, 0.8), (1.6, 2.8) ms. (d) Comparison of 1D ^{11}B skyline projections of the three 2D spectra.*

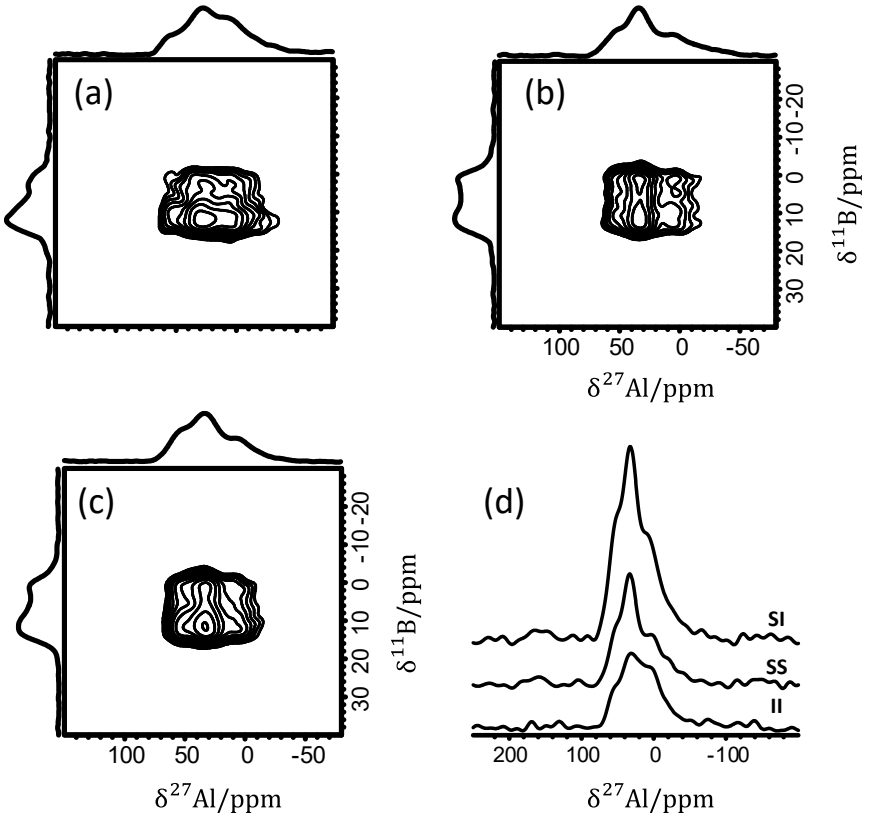

Figure 15. *2D ^{27}Al-^{11}B HETCOR spectra acquired using ^{27}Al{^{11}B} (a) D^{SI}-, (b) D^{SS}- and (c) D^{II}-RINEPT sequences with {τ_1, τ_2} = (1.2, 1.6), (2.8, 1.2), (2.0, 1.6) ms. (d) Comparison of 1D ^{27}Al skyline projections of the three 2D spectra.*

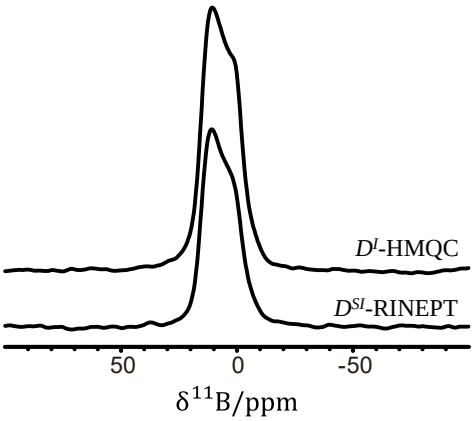

Figure 26. *Comparison of optimal 1D ^{11}B {^{27}Al} D^{I}-HMQC (top) and D^{SI}-RINEPT (bottom) spectra.*

Table 1. *NMR parameters of glass MgO/ 50%B2O3/ 10%Al2O3*

Site	δ_{CS}(ppm)	C_Q(MHz)	T_1(s)	T_2(ms)
$^{11}B_{IV}$	0.67	0.6	~4.1	~12.7
$^{11}B_{III}$	17.0	2.65	~3.8	~21.0
$^{27}Al_{IV}$	64.6	8.3	~1.3	~50
$^{27}Al_{V}$	36.0	7.2	~1.3	~50
$^{27}Al_{VI}$	7.8	6.0	~1.3	~50

Table 2. *Theoretical sensitivities of ^{27}Al-^{11}B D-RINEPT/D-HMQC experiment according to the equation 1.*[a]

Detected nucleus	Excited nucleus	
	^{11}B	^{27}Al
^{11}B	2.50	5.53
^{27}Al	1.00	2.21

a. The FWHM of ^{11}B and ^{27}Al signals of the glass sample are 1280 and 2600 Hz, respectively. The CT enhancement factor ε_{PT} (QFS) of ^{11}B and ^{27}Al are 1.51 and 2.42, respectively. The T_1 of ^{11}B and ^{27}Al nuclei are 4 s and 1.3 s, respectively. The $\boldsymbol{\tau_{RD}}$ of ^{11}B and ^{27}Al nuclei were set 4 and 1 s, respectively. The theoretical sensitivities are normalized with respect to the minimal values in Table 2.

Table S1. Number of scans and t_1 increments as well as t_1 increment and recovery delay for 2D $^{11}B\{^{27}Al\}$ and $^{27}Al\{^{11}B\}$ *D*-HMQC and *D*-RINEPT experiments.

S{*I*}	Scheme	*NS*[a]	N_1[b]	Δt_1 /μs[c]	τ_{RD} /s[d]
$^{11}B\{^{27}Al\}$	*D*-HMQC	128	48	23.83	4
$^{27}Al\{^{11}B\}$		128	48	71.5	1
$^{11}B\{^{27}Al\}$	*D*-RINEPT	128	48	25	1
$^{27}Al\{^{11}B\}$		320	32	100	4

[a] Number of scans. [b] Number of t_1 increments. [c] t_1 increment. [d] Recovery delay.

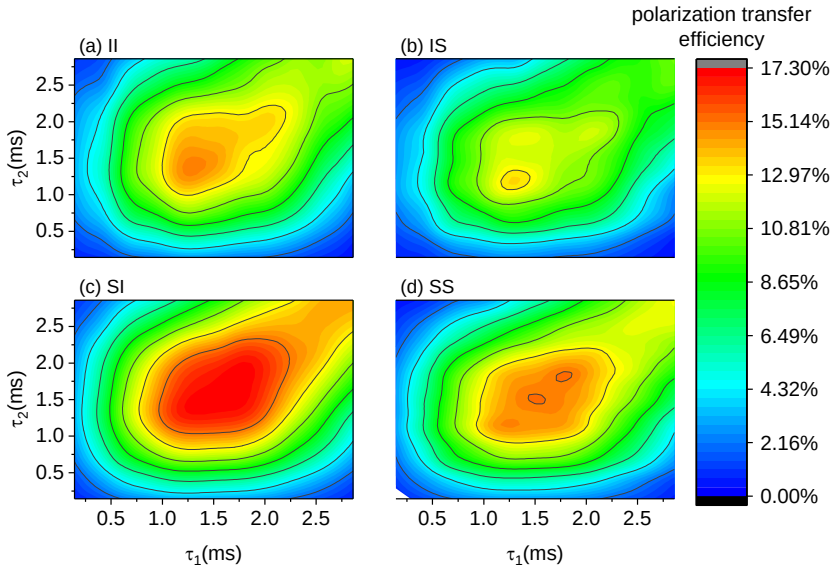

Figure S1 $^{11}B \rightarrow {}^{23}Na$ polarization transfer efficiencies of four ^{23}Na {^{11}B} *D*-RINEPT schemes, *II* (a), *IS* (b), *SI* (c) and *SS*(d), as a function of τ_1 and τ_2. The optimal recoupling time of all schemes are distributed in 1.3-1.6.

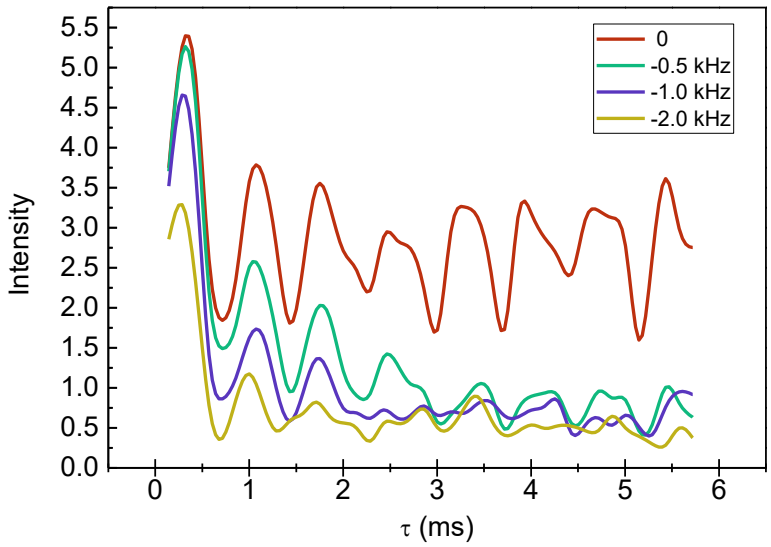

Figure S2. Spin-echo simulations with on an ^{11}B-^{11}B spin pair with different dipolar interactions, 0 kHz (red), 0.5 kHz (cyan), 1 kHz (purple) and 2 kHz (yellow) by using $C2_2^1$recoupling during echo time. The quadrupolar parameters of ^{11}B were C_Q = 2 MHz with η_Q = 0, the RF offset and CSA were neglected in simulations.